Computer Modeling in Engineering & Sciences

Tech Science Press

DOI: 10.32604/cmes.2022.018496

ARTICLE

Numerical Computational Heuristic Through Morlet Wavelet Neural Network for Solving the Dynamics of Nonlinear SITR COVID-19

Zulqurnain Sabir[1], Abeer S. Alnahdi[2,*], Mdi Begum Jeelani[2], Mohamed A. Abdelkawy[2,3,*], Muhammad Asif Zahoor Raja[4], Dumitru Baleanu[5,6] and Muhammad Mubashar Hussain[7]

[1]Department of Mathematics, Hazara University, Mansehra, Pakistan

[2]Department of Mathematics and Statistics, Faculty of Science, Imam Mohammad Ibn Saud Islamic University (IMSIU), Riyadh, Saudi Arabia

[3]Department of Mathematics, Faculty of Science, Beni-Suef University, Beni-Suef, Egypt

[4]Future Technology Research Center, National Yunlin University of Science and Technology, Yunlin, Taiwan

[5]Department of Mathematics, Cankaya University, Ankara, Turkey

[6]Institute of Space Sciences, Magurele-Bucharest, Romania

[7]Department of Mathematics, University of Punjab, Jhelum Campus, Jhelum, Pakistan

[*]Corresponding Authors: Mohamed A. Abdelkawy. Email: maohamed@imamu.edu.sa; Abeer S. Alnahdi. Email: asalnahdi@imamu.edu.sa

Received: 29 July 2021 Accepted: 11 November 2021

ABSTRACT

The present investigations are associated with designing Morlet wavelet neural network (MWNN) for solving a class of susceptible, infected, treatment and recovered (SITR) fractal systems of COVID-19 propagation and control. The structure of an error function is accessible using the SITR differential form and its initial conditions. The optimization is performed using the MWNN together with the global as well as local search heuristics of genetic algorithm (GA) and active-set algorithm (ASA), i.e., MWNN-GA-ASA. The detail of each class of the SITR nonlinear COVID-19 system is also discussed. The obtained outcomes of the SITR system are compared with the Runge-Kutta results to check the perfection of the designed method. The statistical analysis is performed using different measures for 30 independent runs as well as 15 variables to authenticate the consistency of the proposed method. The plots of the absolute error, convergence analysis, histogram, performance measures, and boxplots are also provided to find the exactness, dependability and stability of the MWNN-GA-ASA.

KEYWORDS

Nonlinear SITR model; morlet function; artificial neural networks; Runge-Kutta; treatment; genetic algorithm; treatment; active-set

1 Introduction

Human beings faced many challenges and obstacles, like floods, earthquakes, and viruses, etc. A Few dangerous and spreading diseases are dengue fever produced by the instinctive mosquitos.

It broadly feasts in the African, American, South Asian countries, Oceania regions, Eastern Mediterranean and the Caribbean. It is a kind of perilous and serious virus that wrapped about 0.5 million people each year, but due to the high recovery rate, most of the people get better in a short time. The key indications of the virus are high fever, headache and joint pain. Some other infection base diseases that are hot topics for the researchers are Lassa, Ebola and HIV. To spread and avoid the above infection-based viruses, various medical indications have been extensively applied.

The whole world is now facing coronavirus (COVID-19) that is a deathly, dangerous and spreading disease. This dangerous virus is tremendously transferrable through droplets [1]. The ratio of those individuals that are affected by COVID-19 is so high. At the end of 2019, the first case was reported in the Hubei Province, Wuhan, China [2,3]. Recently, the proper treatment and medicine of the COVID-19 are still not available. However, the vaccination process in some countries is just started to avoid the risk from COVID-19. To avoid COVID-19, different countries did precautionary measures in which lockdown was a common measure. The cases of COVID-19 reported in the whole world mainly in USA, Brazil, India and Europe. The important indications of the COVID-19 are flue, tiredness, fever and dry cough [4]. The COVID-19 badly affected those persons that are suffering some diseases like heart issues, diabetes, chronic respiratory, cardiovascular and cancer. Those who feel these symptoms of dry cough, breathing difficulty, flue and high temperature, should directly contact the doctor.

The SITR fractal model basis on the COVID-19 is dependent upon four classes, 'susceptible (S_1 and S_2)', 'infected (I)', 'treatment (T)' and 'recovered (R)', mathematically written as [5]:

$$\begin{cases} S_1'(\Omega) = -\delta\beta T(\Omega) - (\alpha + \beta I(\Omega)) S_1(\Omega) + B, & S_1(0) = b_1, \\ S_2'(\Omega) = -\delta\beta T(\Omega) - (\alpha + \beta I(\Omega)) S_2(\Omega) + B, & S_2(0) = b_2, \\ I'(\Omega) = -(-\sigma + \alpha + \mu) I(\Omega) + \beta (S_1(\Omega) + S_2(\Omega)) I(\Omega) + \beta\delta T(\Omega), & I(0) = b_3, \\ T'(\Omega) = (\psi - \rho + \varepsilon - \alpha) T(\Omega) + \mu I(\Omega), & T(0) = b_4, \\ R'(\Omega) = \rho T(\Omega) - \alpha R(\Omega), & R(0) = b_5, \end{cases} \tag{1}$$

where $S_1(\Omega)$ and $S_2(\Omega)$ are both uninfected class from COVID-19 of young people and older or have serious diseases, $I(\Omega)$ is the class shows the infected people from coronavirus, $T(\Omega)$ is the treatment and $R(\Omega)$ is the recovered class. The detailed parameters are defined in Table 1.

Table 1: Parameter's demonstrations of the SITR model

Parameter	Description
ε	Rate of sleep factor
ρ	Infection ratio
B	Natural birth rate
μ	Recovery rate
ψ	Ratio of healthy food
α	Death rate
σ	Corona symptoms rate
δ	Infection reduced by treatment
β	Contact rate
b_l, $l = 1, 2 \ldots, 5$	Initial conditions

This research aimsto solve the SITR fractal model of COVID-19 by designing the Morlet wavelet neural network (MWNN) along with the optimization of global and local search heuristics of genetic algorithm (GA) and active-set algorithm (ASA), i.e., MWNN-GA-ASA. The authors are inspired to solve the nonlinear COVID-19 fractal model by applying the proposed method due to the immense applications of stochastic computing solvers. Few of them are nonlinear singular delay differential model [6,7], multi-fractional multi-singular differential models [8–10], fractional-order pantograph Lane-Emden differential systems [11], prey-predator models [12], second grade nanofluidic system [13], heat transfer possessions in a Bodewadt flow [14], solution of functionally graded material of the porous fin model [15], HIV infection system [16], hybrid hydro-nanofluid Al_2O_3–Cu–H_2O model [17], Ferrofluidic models [18], singular functional systems [19], magnetohydrodynamic squeezing flow model [20], Cattaneo-christov heat flux model [21], nonlinear optics [22], nonlinear Falkner-Skan systems [23], singular Thomas-Fermi system [24], thin-film flow of Maxwell nanofluidic model [25], mosquito dispersal nonlinear system [26], nonlinear corneal shape model [27], heat conduction based human head system [28], mathematical model for entropy generation system [29] and singular periodic models [30,31]. The novel features of the MWNN-GA-ASA are given as:

- The design of MWNN is presented effectively to solve the nonlinear SITR fractal system of equations.
- The proposed MWNN-GA-ASA is implemented effectively to solve the nonlinear dynamics of the COVID-19 fractal model.
- Authentication of the performance through MWNN-GA-ASA is verified by overlapping the proposed results with the Runge-kutta solutions.
- The absolute error (AE) to solve the SITR fractal model is obtained in good measures to demonstrate the worth of the designed method.
- The reliability of the proposed method is observed using the statistical measures to solve the SITR fractal model.

The rest of the paper's parts are given as: Section 2 shows the methodology based on MWNN-GA-ASA and performance indices. Section 3 describes the results and discussions of the nonlinear SITR fractal model. The concluding remarks and future research directions are given in the last section.

2 Methodology

The designed procedures to solve the SITR fractal model is described in two parts:

1. Introduce a fitness function.
2. The optimization procedures of GA-ASA are described.

2.1 ANN Modeling

The representations of the systems given in (1) based on the continuous ANNs mapping to get the performances of each class of the model and its derivatives are given as:

$$\begin{bmatrix} \hat{S}_1(\Omega), \hat{S}_2(\Omega), \\ \hat{I}(\Omega), \quad \hat{T}(\Omega), \\ \hat{R}(\Omega) \end{bmatrix} = \begin{bmatrix} \sum_{p=1}^{m} u_{S_1,p} L\left(w_{S_1,p}\Omega + v_{S_1,p}\right), \sum_{p=1}^{m} u_{S_2,p} L\left(w_{S_2,p}\Omega + v_{S_2,p}\right), \\ \sum_{p=1}^{m} u_{I,p} L\left(w_{I,p}\Omega + v_{I,p}\right), \quad \sum_{p=1}^{m} u_{T,p} L\left(w_{T,p}\Omega + v_{T,p}\right), \\ \sum_{p=1}^{m} u_{R,p} L\left(w_{R,p}\Omega + v_{R,p}\right) \end{bmatrix}, \tag{2}$$

$$\begin{bmatrix} \hat{S}'_1(\Omega), \hat{S}'_2(\Omega), \\ \hat{I}'(\Omega), \hat{T}'(\Omega), \\ \hat{R}'(\Omega) \end{bmatrix} = \begin{bmatrix} \sum_{p=1}^{m} u_{S_1,p} L'\left(w_{S_1,p}\Omega + v_{S_1,p}\right), \sum_{k=1}^{m} u_{S_2,p} L'\left(w_{S_2,p}\Omega + v_{S_2,p}\right), \\ \sum_{p=1}^{m} u_{I,p} L'\left(w_{I,p}\Omega + v_{I,p}\right), \sum_{k=1}^{m} u_{T,p} L'\left(w_{T,p}\Omega + v_{T,p}\right), \\ \sum_{p=1}^{m} u_{R,p} L'\left(w_{R,p}\Omega + v_{R,p}\right) \end{bmatrix},$$

where W is the unknown weight vector and is to be calculated, given as:

$$\boldsymbol{W} = \begin{bmatrix} \boldsymbol{W}_{S_1} \\ \boldsymbol{W}_{S_2} \\ \boldsymbol{W}_I \\ \boldsymbol{W}_T \\ \boldsymbol{W}_R \end{bmatrix}^t \quad \boldsymbol{W}_{S_1} = \begin{bmatrix} \boldsymbol{u}_{S_1} \\ \boldsymbol{w}_{S_1} \\ \boldsymbol{v}_{S_1} \end{bmatrix}^t, \ \boldsymbol{W}_{S_2} = \begin{bmatrix} \boldsymbol{u}_{S_2} \\ \boldsymbol{w}_{S_2} \\ \boldsymbol{v}_{S_2} \end{bmatrix}^t, \ \boldsymbol{W}_I = \begin{bmatrix} \boldsymbol{u}_I \\ \boldsymbol{w}_I \\ \boldsymbol{v}_I \end{bmatrix}^t, \ \boldsymbol{W}_T = \begin{bmatrix} \boldsymbol{u}_T \\ \boldsymbol{w}_T \\ \boldsymbol{v}_T \end{bmatrix}^t, \ \boldsymbol{W}_R = \begin{bmatrix} \boldsymbol{u}_R \\ \boldsymbol{w}_R \\ \boldsymbol{v}_R \end{bmatrix}^t.$$

where

$$\boldsymbol{u}_{S_1} = \left[u_{S_1,1}, u_{S_1,2}, u_{S_1,3}, \ldots, u_{S_1,m}\right], \quad \boldsymbol{u}_{S_2} = \left[u_{S_2,1}, u_{S_2,2}, u_{S_2,3}, \ldots, u_{S_2,m}\right],$$
$$\boldsymbol{u}_I = \left[u_{I,1}, \ u_{I,2}, \ u_{I,3}, \ldots, \ u_{I,m}\right] \quad \boldsymbol{u}_T = \left[u_{T,1}, u_{T,2}, \ u_{T,3}, \ldots, u_{T,m}\right],$$
$$\boldsymbol{u}_R = \left[u_{R,1}, \ u_{R,2}, u_{R,3}, \ldots, \ u_{R,m}\right], \quad \boldsymbol{\omega}_{S_1} = \left[w_{S_1,1}, w_{S_1,2}, w_{S_1,3}, \ldots, w_{S_1,m}\right],$$
$$\boldsymbol{\omega}_{S_2} = \left[w_{S_2,1}, w_{S_2,2}, w_{S_2,3}, \ldots, w_{S_2,m}\right], \quad \boldsymbol{\omega}_I = \left[w_{I,1}, \ w_{I,2}, w_{I,3}, \ldots, w_{I,m}\right],$$
$$\boldsymbol{\omega}_T = \left[w_{T,1}, w_{T,2}, \ w_{T,3}, \ldots, \ w_{T,m}\right], \quad \boldsymbol{\omega}_R = \left[w_{R,1}, w_{R,2}, w_{R,3}, \ldots, w_{R,m}\right],$$
$$\boldsymbol{v}_{S_1} = \left[v_{S_1,1}, v_{S_1,2}, v_{S_1,3}, \ldots, \ v_{S_1,m}\right], \quad \boldsymbol{v}_{S_2} = \left[v_{S_2,1}, \ v_{S_2,2}, \ v_{S_2,3}, \ldots, v_{S_2,m}\right],$$
$$\boldsymbol{v}_I = \left[v_{I,1}, \ v_{I,2}, \ v_{I,3}, \ldots, \ v_{I,m}\right], \quad \boldsymbol{v}_T = \left[v_{T,1}, \ v_{T,2}, \ v_{T,3}, \ldots, \ v_{T,m}\right],$$
$$\boldsymbol{v}_R = \left[v_{R,1}, \ v_{R,2}, \ v_{R,3}, \ldots, \ v_{R,m}\right].$$

The MWNN is not applied before for solving the SITR fractal model, mathematically MW function is written as [32–34]:

$$L(\Omega) = \cos(1.75\Omega)\, e^{-0.5\Omega^2}.$$

$$\begin{bmatrix} \hat{S}_1(\Omega), \hat{S}_2(\Omega), \hat{I}(\Omega), \\ \hat{R}(\Omega), \hat{T}(\Omega) \end{bmatrix} = \begin{bmatrix} \sum_{p=1}^{m} u_{S_1,p} \cos\left(1.75\left(w_{S_1,p}\Omega + v_{S_1,p}\right)\right) e^{-0.5\left(w_{S_1,p}\Omega + v_{S_1,p}\right)^2}, \\ \sum_{p=1}^{m} u_{S_2,p} \cos\left(1.75\left(w_{S_2,p}\Omega + v_{S_2,p}\right)\right) e^{-0.5\left(w_{S_2,p}\Omega + v_{S_2,p}\right)^2}, \\ \sum_{p=1}^{m} u_{I,p} \cos\left(1.75\left(w_{I,p}\Omega + v_{I,p}\right)\right) e^{-0.5\left(w_{I,p}\Omega + v_{I,p}\right)^2}, \\ \sum_{p=1}^{m} u_{T,p} \cos\left(1.75\left(w_{T,p}\Omega + v_{T,p}\right)\right) e^{-0.5\left(w_{T,p}\Omega + v_{T,p}\right)^2}, \\ \sum_{p=1}^{m} u_{R,p} \cos\left(1.75\left(w_{R,p}\Omega + v_{R,p}\right)\right) e^{-0.5\left(w_{R,p}\Omega + v_{R,p}\right)^2}, \end{bmatrix}, \tag{3}$$

$$\begin{bmatrix} \hat{S}'_1(\Omega), \hat{S}'_2(\Omega), \hat{I}'(\Omega), \\ \hat{R}'(\Omega), \hat{T}'(\Omega) \end{bmatrix} = \frac{d}{d\Omega} \begin{bmatrix} \sum_{k=1}^{m} u_{S_1,p} \cos\left(1.75\left(w_{S_1,p}\Omega + v_{S_1,p}\right)\right) e^{-0.5\left(w_{S_1,p}\Omega + v_{S_1,p}\right)^2}, \\ \sum_{k=1}^{m} u_{S_2,p} \cos\left(1.75\left(w_{S_2,p}\Omega + v_{S_2,p}\right)\right) e^{-0.5\left(w_{S_2,p}\Omega + v_{S_2,p}\right)^2}, \\ \sum_{k=1}^{m} u_{I,p} \cos\left(1.75\left(w_{I,p}\Omega + v_{I,p}\right)\right) e^{-0.5\left(w_{I,p}\Omega + v_{I,p}\right)^2}, \\ \sum_{k=1}^{m} u_{T,p} \cos\left(1.75\left(w_{T,p}\Omega + v_{T,p}\right)\right) e^{-0.5\left(w_{T,p}\Omega + v_{T,p}\right)^2}, \\ \sum_{k=1}^{m} u_{R,p} \cos\left(1.75\left(w_{R,p}\Omega + v_{R,p}\right)\right) e^{-0.5\left(w_{R,p}\Omega + v_{R,p}\right)^2}, \end{bmatrix}.$$

Using the above network, the objective function takes the form as:

$$\xi = \xi_1 + \xi_2 + \xi_3 + \xi_4 + \xi_5 + \xi_6, \tag{4}$$

$$\xi_1 = \frac{1}{N}\sum_{p=1}^{N}\left(\left(\widehat{S'}_1\right)_p + \left(\beta\hat{I}_p + \alpha\right)\left(\hat{S}_1\right)_p + \delta\beta\hat{T}_p - B\right)^2, \tag{5}$$

$$\xi_2 = \frac{1}{N}\sum_{p=1}^{N}\left(\left(\widehat{S'}_2\right)_p + \left(\beta\hat{I}_p + \alpha\right)\left(\hat{S}_2\right)_p + \delta\beta\hat{T}_p - B\right)^2, \tag{6}$$

$$\xi_3 = \frac{1}{N}\sum_{p=1}^{N}\left(\hat{I'}_k - \left(\left(\hat{S}_1\right)_p + \left(\hat{S}_2\right)_p\right)\beta\hat{I}_p + (\alpha - \sigma + \mu)\hat{I}_p - \beta\delta\hat{T}_p\right)^2, \tag{7}$$

$$\xi_4 = \frac{1}{N}\sum_{p=1}^{N}\left(\hat{T'}_p - \mu\hat{I}_p - (\varepsilon - \rho - \alpha + \psi)\hat{T}_p\right)^2, \tag{8}$$

$$\xi_5 = \frac{1}{N}\sum_{p=1}^{N}\left(\hat{R'}_p + \alpha\hat{R}_p - \rho\hat{T}_p\right)^2, \tag{9}$$

$$\xi_6 = \frac{1}{5}\left(\left(\left(\hat{S}_1\right)_0 - b_1\right)^2 + \left(\left(\hat{S}_2\right)_0 - b_2\right)^2 + \left(\hat{I}_0 - b_3\right)^2 + \left(\hat{T}_0 - b_4\right)^2 + \left(\hat{R}_0 - b_5\right)^2\right), \tag{10}$$

where $\Omega_p = ph, \left(\hat{S}_1\right)_p = \hat{S}_1(\Omega_p), \left(\hat{S}_2\right)_p = \hat{S}_2(\Omega_p)$, $\hat{I}_p = \hat{I}(\Omega_p)$, $\hat{T}_p = \hat{T}(\Omega_p)$, $Nh = 1$ and $\hat{R}_p = \hat{R}(\Omega_p)$. The proposed results for each class of the nonlinear SITR fractal model are defined as $\hat{S}_1(\Omega)$, $\hat{S}_2(\Omega)$, $\hat{I}(\Omega)$, $\hat{T}(\Omega)$ and $\hat{R}(\Omega)$. Similarly, ξ_1, ξ_2, ξ_3, ξ_4, ξ_5 and ξ_6 indicate the objective functions using the differential forms and initial conditions.

2.2 Optimization: GA-ASA

The detail of GA-ASA is provided to optimize the error function based on the COVID-19 nonlinear system is provided in this section.

GA is known as a global search procedure applied broadly to solve constrained and unconstrained problems. GA works through the procedures of crossover, selection, elitism and mutation operators. In recent, GA is executed in lung cancer prognosis [35], wellhead backpressure control system [36], nonlinear circuits [37], heterogeneous mosquito release ecosystem [38], active noise control systems [39], multi-fractional multi-singular singular model [40], gas tungsten arc welding process [41], adjusting sensor acquisition frequency [42], multilayer piezoelectric transducer for broadband structures [43] and singular nonlinear system [44].

The process of GA converges rapidly to hybridize with the appropriate local search method by taking the best values of GA as an initial input. Consequently, an effective local ASA is implemented to adjust the outcomes of the global search procedure. Recently, ASA is used in pricing American better-of option [45], non-smooth large-scale optimization systems with box constraints [46], regularized monotonic regression [47], cardiac defibrillation [48], multivariate integration under modest error demand [49] and predictive control for a ball and beam system [50]. The present investigations are associated to solve the SITR fractal model using the GA-ASA hybridization. The comprehensive detail of MWNN-GA-ASA is provided in the pseudocode-based Table 2.

Table 2: Optimization performance to solve the SITR fractal model

Start GA

[Inputs]: For the equal number of network's element, the chromosomes are measured as: of the network as:

$W = [\boldsymbol{u},\boldsymbol{w},\boldsymbol{v}]$

Population: Set of chromosomes is provided as:

$$\boldsymbol{W} = \begin{bmatrix} \boldsymbol{W}_{S_1} \\ \boldsymbol{W}_{S_2} \\ \boldsymbol{W}_I \\ \boldsymbol{W}_T \\ \boldsymbol{W}_R \end{bmatrix}^t, \text{ where } \boldsymbol{W}_{S_1} = \begin{bmatrix} \boldsymbol{u}_{S_1} \\ \boldsymbol{w}_{S_1} \\ \boldsymbol{v}_{S_1} \end{bmatrix}^t, \boldsymbol{W}_{S_2} = \begin{bmatrix} \boldsymbol{u}_{S_2} \\ \boldsymbol{w}_{S_2} \\ \boldsymbol{v}_{S_2} \end{bmatrix}^t, \boldsymbol{W}_I = \begin{bmatrix} \boldsymbol{u}_I \\ \boldsymbol{w}_I \\ \boldsymbol{v}_I \end{bmatrix}^t, \boldsymbol{W}_T = \begin{bmatrix} \boldsymbol{u}_T \\ \boldsymbol{w}_T \\ \boldsymbol{v}_T \end{bmatrix}^t,$$

$$\boldsymbol{W}_R = \begin{bmatrix} \boldsymbol{u}_R \\ \boldsymbol{w}_R \\ \boldsymbol{v}_R \end{bmatrix}^t$$

Output: $W_{\textbf{GA-Best}}$ signifies the weights based on global vectors.

Initialization: For the assortment of chromosomes, regulate the $W_{\textbf{GA-Best}}$.

Fit Assessment: Amend Fitness ξ) in the population (P) using Eqs. (4)–(8).

- **Stopping standards:** Stop, if [iterations = 30], [$\xi = 10^{-22}$], [TolCon = 10^{-20}], [StallLimit = 120], [TolFun = 10^{-23}] & [PopSize = 210]

(Continued)

Table 2 (Continued)

Move to **[storage]**
Ranking: Rank $W_{\text{GA-Best}}$ in P for ξ.
Storage: Store $W_{\text{GA-Best}}$, ξ, generations, function count & time for the values of GA.
End of GA
ASA Starts
Inputs: $W_{\text{GA-Best}}$ is starting point.
Output: $W_{\text{GA-ASA}}$ is the best weight vector of GA-ASA.
Initialize: $W_{\text{GA-Best}}$, Iterations & Assignments.
Terminating standards: Stop, if [TolX $= 10^{-20}$], [$\xi = 10^{-22}$], [TolFun $= 10^{-21}$], [Iterations $= 150$] & [MaxFunEvals $= 230000$].
FIT approximation: Compute $W_{\text{GA-ASA}}$ and ξ using Eqs. (4)–(8).
Amendments: Regulate 'fmincon' for ASA, ξ to improve the '**W**' for Eqs. (4)–(8).
Store: Transmute $W_{\text{GA-ASA}}$, ξ, iterations, function counts, and time.
ASA End

3 Performance Indices

The mathematical performances of the mean absolute deviation (MAD), variance account for (V.A.F) and Theil's inequality coefficient (T.I.C) are provided to solve the nonlinear SITR fractal model, given as:

$$\begin{bmatrix}\text{MAD}_{S_1}, \text{MAD}_{S_2}, \text{MAD}_I, \\ \text{MAD}_T, \text{MAD}_R\end{bmatrix} = \begin{bmatrix}\frac{1}{n}\sum_{p=1}^{n}\left|\left((S_1)_p - \left(\hat{S}_1\right)_p\right)\right|, \frac{1}{n}\sum_{p=1}^{n}\left|\left((S_2)_p - \left(\hat{S}_2\right)_p\right)\right|, \frac{1}{n}\sum_{p=1}^{n}\left|\left(I_p - \hat{I}_p\right)\right|, \\ \frac{1}{n}\sum_{p=1}^{n}\left|\left(T_p - \hat{T}_p\right)\right|, \frac{1}{n}\sum_{p=1}^{n}\left|\left(R_p - \hat{R}_p\right)\right|\end{bmatrix} \tag{11}$$

$$\begin{cases}\begin{bmatrix}\text{VAF}_{S_1}, \text{VAF}_{S_2}, \\ \text{VAF}_I, \text{VAF}_T, \\ \text{VAF}_R\end{bmatrix} = \begin{bmatrix}\left(1 - \frac{\text{var}\left((S_1)_p - \left(\hat{S}_1\right)_p\right)}{\text{var}\,(S_1)_p}\right) \times 100, \left(1 - \frac{\text{var}\left((S_2)_p - \left(\hat{S}_2\right)_p\right)}{\text{var}\,(S_2)_p}\right) \times 100, \\ \left(1 - \frac{\text{var}\left(I_p - \hat{I}_p\right)}{\text{var}\left(I_p\right)}\right) \times 100, \quad \left(1 - \frac{\text{var}\left(T_p - \hat{T}_p\right)}{\text{var}\left(T_p\right)}\right) \times 100, \\ \left(1 - \frac{\text{var}\left(R_p - \hat{R}_p\right)}{\text{var}\left(R_p\right)}\right) \times 100,\end{bmatrix} \\ \left[\text{EVAF}_{S_1}, \text{EVAF}_{S_2}, \text{EVAF}_I, \text{EVAF}_T, \text{EVAF}_R\right] = \begin{bmatrix}\left|100 - \text{VAF}_{S_1}, 100 - \text{VAF}_{S_2}, 100 - \text{VAF}_I, \right| \\ \left|100 - \text{VAF}_T, 100 - \text{VAF}_R\right|\end{bmatrix}.\end{cases} \tag{12}$$

$$\begin{bmatrix} \mathrm{TIC}_{S_1}, \mathrm{TIC}_{S_2}, \\ \mathrm{TIC}_I, \mathrm{TIC}_T, \\ \mathrm{TIC}_R \end{bmatrix} = \begin{bmatrix} \dfrac{\sqrt{\frac{1}{n}\sum_{p=1}^{n}\left((S_1)_p - \left(\hat{S}_1\right)_p\right)^2}}{\left(\sqrt{\frac{1}{n}\sum_{p=1}^{n}(S_1)_p^2} + \sqrt{\frac{1}{n}\sum_{p=1}^{n}\left(\hat{S}_1\right)_p^2}\right)}, & \dfrac{\sqrt{\frac{1}{n}\sum_{p=1}^{n}\left((S_2)_p - \left(\hat{S}_2\right)_p\right)^2}}{\left(\sqrt{\frac{1}{n}\sum_{p=1}^{n}(S_2)_p^2} + \sqrt{\frac{1}{n}\sum_{p=1}^{n}\left(\hat{S}_2\right)_p^2}\right)}, \\ \dfrac{\sqrt{\frac{1}{n}\sum_{k=1}^{n}\left(I_p - \hat{I}_p\right)^2}}{\left(\sqrt{\frac{1}{n}\sum_{p=1}^{n}I_p^2} + \sqrt{\frac{1}{n}\sum_{p=1}^{n}\hat{I}_p^2}\right)}, & \dfrac{\sqrt{\frac{1}{n}\sum_{p=1}^{n}\left(T_p - \hat{T}_p\right)^2}}{\left(\sqrt{\frac{1}{n}\sum_{p=1}^{n}T_p^2} + \sqrt{\frac{1}{n}\sum_{p=1}^{n}\hat{T}_p^2}\right)}, \\ \dfrac{\sqrt{\frac{1}{n}\sum_{p=1}^{n}\left(R_p - \hat{R}_p\right)^2}}{\left(\sqrt{\frac{1}{n}\sum_{p=1}^{n}R_p^2} + \sqrt{\frac{1}{n}\sum_{p=1}^{n}\hat{R}_p^2}\right)} & \end{bmatrix}. \quad (13)$$

4 Results and Discussion

In this section, the detail to solve the nonlinear SITR fractal is provided. The comparative studies using the Runge-Kutta numerical solutions designates the accuracy of MWNN-GA-ASA. Furthermore, statistical assessments express the precision of the proposed method to solve the nonlinear SITR fractal system.

4.1 SITR Fractal System

The suitable values of the parameter are provided in Table 3 and a simplified form of the model is given as:

Table 3: Descriptions, indexes and allocated suitable measures for the nonlinear SITR mathematical model

Symbol	Description	Values
ε	Rate of sleep factor	0.1
ρ	Infection ratio	0.29
B	Natural birth rate	0.3
μ	Recovery rate	0.1
ψ	Ratio of healthy food	0.2
α	Death rate	0.25
σ	Corona symptoms rate	0.005
δ	Infection reduced by treatment	0.3
β	Contact rate	0.35

The updated form of the nonlinear SITR model (1) using the above Table 3 values are written as:

$$\begin{cases} S_1'(\Omega) = 0.3 - 0.105T(\Omega) - (0.35I(\Omega) + 0.25)S_1(\Omega), & S_1(0) = 0.65, \\ S_2'(\Omega) = 0.3 - 0.105T(\Omega) - (0.35I(\Omega) + 0.25)S_2(\Omega), & S_2(0) = 0.15, \\ I'(\Omega) = 0.105T(\Omega) + 0.35I(\Omega)(S_1(\Omega) + S_2(\Omega)) - 0.345I(\Omega), & I(0) = 0.75, \\ T'(\Omega) = -0.25T(\Omega) + 0.1I(\Omega), & imtT(0) = 0.35, \\ R'(\Omega) = -0.25R(\Omega) + 0.3T(\Omega), & R(0) = 0.1, \end{cases} \tag{14}$$

The objective function of the above system is shown as:

$$\xi = \frac{1}{N}\sum_{k=1}^{N}\left(\begin{array}{l} \left[\left(\widehat{S'}_1\right)_p - 0.3 + \left(0.25 + 0.35\hat{I}_p\right)\left(\hat{S}_1\right)_p + 0.105\hat{T}_p\right]^2 + \\ \left[\left(\widehat{S'}_2\right)_p - 0.3 + \left(0.25 + 0.35\hat{I}_p\right)\left(\hat{S}_2\right)_p + 0.105\hat{T}_p\right]^2 + \\ \left[\hat{I'}_p + 0.345\hat{I}_p - 0.35\hat{I}_p\left(\left(\hat{S}_1\right)_p + \left(\hat{S}_2\right)_p\right) - 0.105\hat{T}_p\right]^2 + \\ \left[\hat{T'}_p + 0.25\hat{T}_p - 0.1\hat{I}_p\right]^2 + \left[\hat{R'}_p + 0.25\hat{R}_p - 0.3\hat{T}_p\right]^2 \end{array}\right) + \tag{15}$$

$$0.2\left(\left((\hat{S}_1)_0 - \frac{65}{100}\right)^2 + \left((\hat{S}_2)_0 - \frac{15}{100}\right)^2 + \left(\hat{T}_0 - \frac{35}{100}\right)^2 + \left(\hat{I}_0 - \frac{75}{100}\right)^2 + \left(\hat{R}_0 - \frac{1}{10}\right)^2\right)$$

The optimization of the SITR fractal model is achieved with the competency of GA-ASA for 30 runs along with 5 neurons. The MWNN-GA-ASA structure for solving the SITR fractal system is displayed in Fig. 1. The values of the best weight sets are given in Fig. 2. These vectors are accomplished for the proposed outcomes of the nonlinear SITR fractal model. The estimated outcomes for each class of the nonlinear SITR fractal system based on MWNN-GA-ASA are written as:

$$\begin{aligned} \hat{S}_1(\Omega) = {} & -0.089\cos(1.75(0.7998\Omega + 0.7588))e^{-0.5(0.7998\Omega+0.7588)^2} \\ & -0.1478\cos(1.75(0.0508\Omega + 1.3378))e^{-0.5(0.0508\Omega+1.3378)^2} \\ & +0.1373\cos(1.75(-0.051\Omega + 0.7000))e^{-0.5(-0.051\Omega+0.7000)^2} \\ & -0.7340\cos(1.75(0.6862\Omega - 1.9474))e^{-0.5(0.6862\Omega-1.9474)^2} \\ & +0.4902\cos(1.75(0.1306\Omega + 0.0353))e^{-0.5(0.1306\Omega+0.0353)^2}, \end{aligned} \tag{16}$$

$$\begin{aligned} \hat{S}_2(\Omega) = {} & 1.0291\cos(1.75(1.5158\Omega + 3.5529))e^{-0.5(1.5158\Omega+3.5529)^2} \\ & -0.7151\cos(1.75(-1.474\Omega - 3.4331))e^{-0.5(-1.474\Omega-3.4331)^2} \\ & +1.2637\cos(1.75(-0.163\Omega - 2.0456))e^{-0.5(-0.163\Omega-2.0456)^2} \\ & +0.1519\cos(1.75(0.6111\Omega + 2.3225))e^{-0.5(0.6111\Omega+2.3225)^2} \\ & -1.3470\cos(1.75(-0.136\Omega - 1.1502))e^{-0.5(-0.136\Omega-1.1502)^2}, \end{aligned} \tag{17}$$

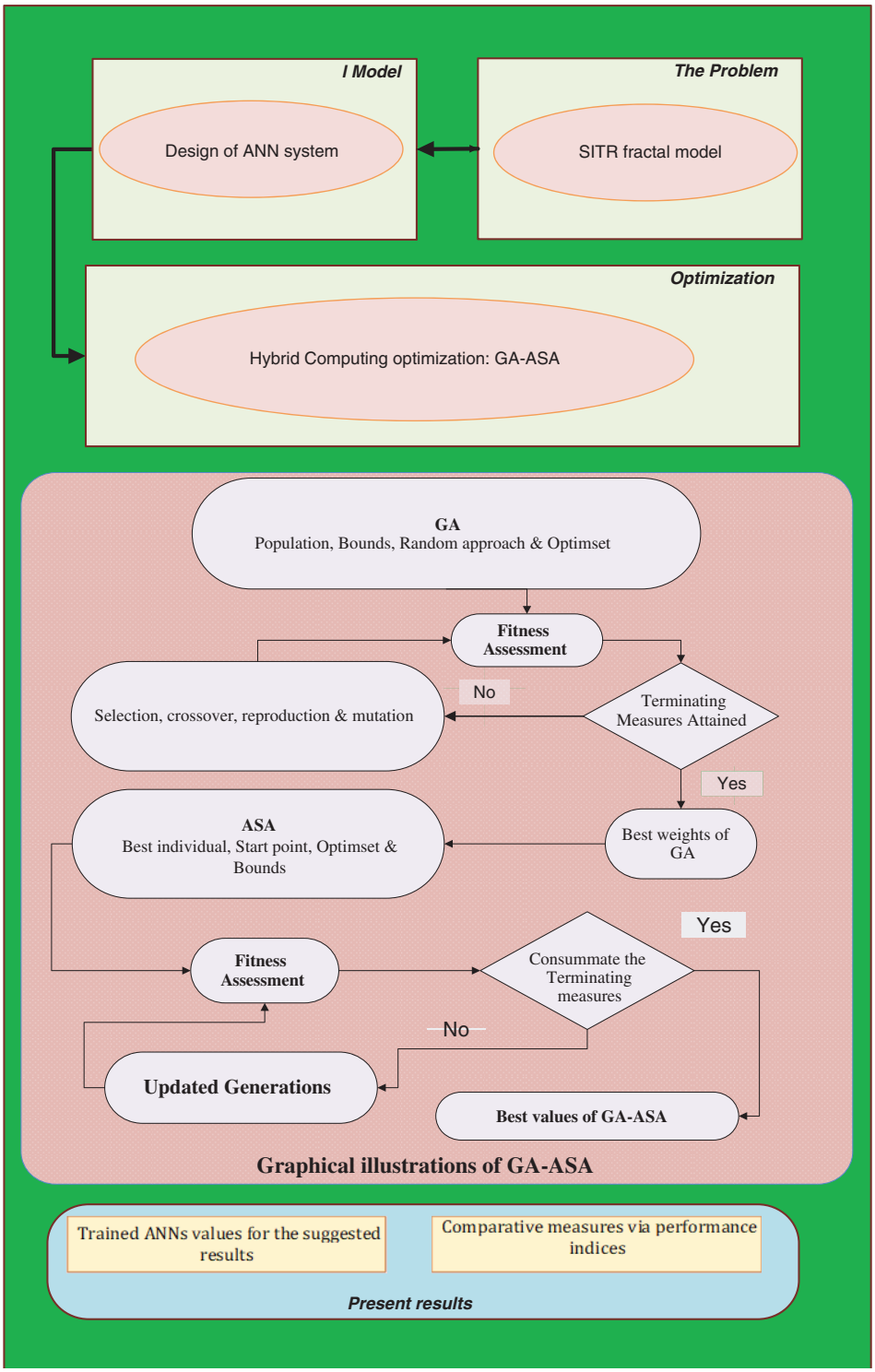

Figure 1: MWNN-GA-ASA structure to solve the SITR fractal system

$$\begin{aligned}\hat{I}(\Omega) = {} & 0.8550\cos(1.75(0.2532\Omega - 1.0049))e^{-0.5(0.2532\Omega-1.0049)^2} \\ & -0.5164\cos(1.75(-0.123\Omega - 1.4089))e^{-0.5(-0.123\Omega-1.4089)^2} \\ & -1.2719\cos(1.75(-0.075\Omega - 1.7133))e^{-0.5(-0.075\Omega-1.7133)^2} \\ & -0.1673\cos(1.75(-0.427\Omega - 1.3354))e^{-0.5(-0.427\Omega-1.3354)^2} \\ & -1.2935\cos(1.75(0.0244\Omega - 1.5146))e^{-0.5(0.0244\Omega-1.5146)^2},\end{aligned} \tag{18}$$

$$\begin{aligned}\hat{T}(\Omega) = {} & -0.032\cos(1.75(0.6127\Omega + 1.7895))e^{-0.5(0.6127\Omega+1.7895)^2} \\ & +0.0462\cos(1.75(1.1673\Omega + 2.7581))e^{-0.5(1.1673\Omega+2.7581)^2} \\ & -0.0709\cos(1.75(-0.393\Omega - 1.2088))e^{-0.5(-0.393\Omega-1.2088)^2} \\ & +0.3425\cos(1.75(0.0104\Omega + 0.1428))e^{-0.5(0.0104\Omega+0.1428)^2} \\ & -0.1518\cos(1.75(-0.133\Omega + 1.7493))e^{-0.5(-0.133\Omega+1.7493)^2},\end{aligned} \tag{19}$$

$$\begin{aligned}\hat{R}(\Omega) = {} & 3.0081\cos(1.75(0.1771\Omega + 2.2652))e^{-0.5(0.1771\Omega+2.2652)^2} \\ & -0.0314\cos(1.75(-0.331\Omega - 0.9404))e^{-0.5(-0.331\Omega-0.9404)^2} \\ & +0.1390\cos(1.75(-0.125\Omega + 0.6440))e^{-0.5(-0.125\Omega+0.6440)^2} \\ & +0.1945\cos(1.75(0.1036\Omega - 0.7206))e^{-0.5(0.1036\Omega-0.7206)^2} \\ & +0.0182\cos(1.75(-0.430\Omega - 0.7343))e^{-0.5(-0.430\Omega-0.7343)^2},\end{aligned} \tag{20}$$

The systems of Eqs. (16)–(20) are provided to evaluate the solutions of the nonlinear SITR fractal model and the outcomes are illustrated in the Figs. 2–5 using 15 variables or 5 neurons. Fig. 2 shows the trained weights set for the nonlinear coronavirus model. Fig. 3 illustrates the best, mean and proposed results based on the nonlinear SITR fractal model. It is noted that the best, mean and proposed solutions od the model overlapped to each other. Fig. 4 signifies the AE values and it is observed that the performances of the SITR fractal model that lie around 10^{-04}–10^{-06}, 10^{-03}–10^{-05}, 10^{-04}–10^{-07}, 10^{-05}–10^{-06} and 10^{-05}–10^{-08}. The mean performances of the SITR fractal model are calculated around 10^{-01}–10^{-02}. It is observed on the behalf of the AE that the proposed computational approach is accurate to solve the coronavirus model.

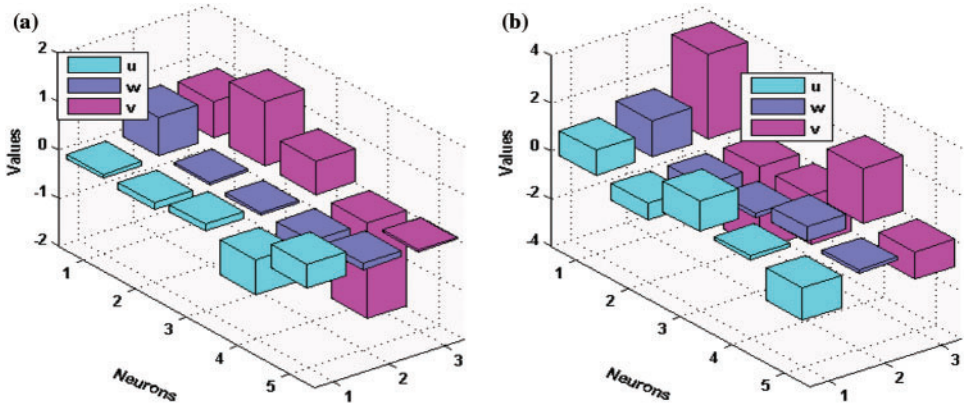

Figure 2: (Continued)

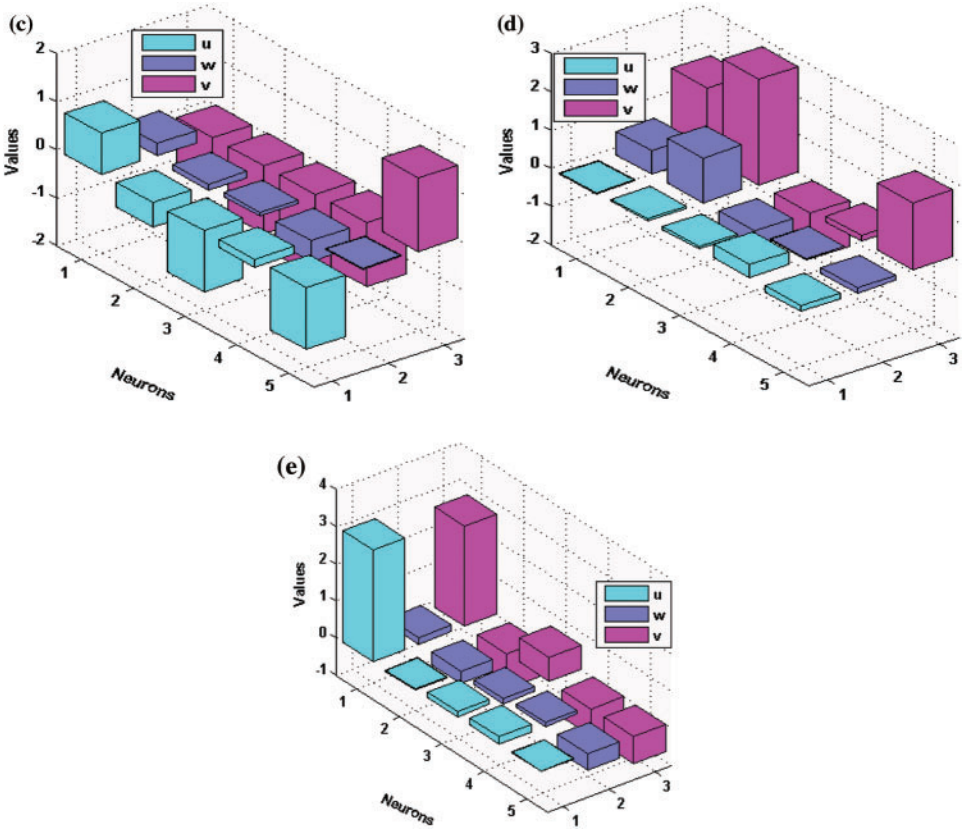

Figure 2: Best weights set for the SITR fractal system (a) Best weights for the class S_1 (b) Best weight for the class S_2 (c) Best weight for the class I (d) Best weight for the class T (e) Best weight for the class R

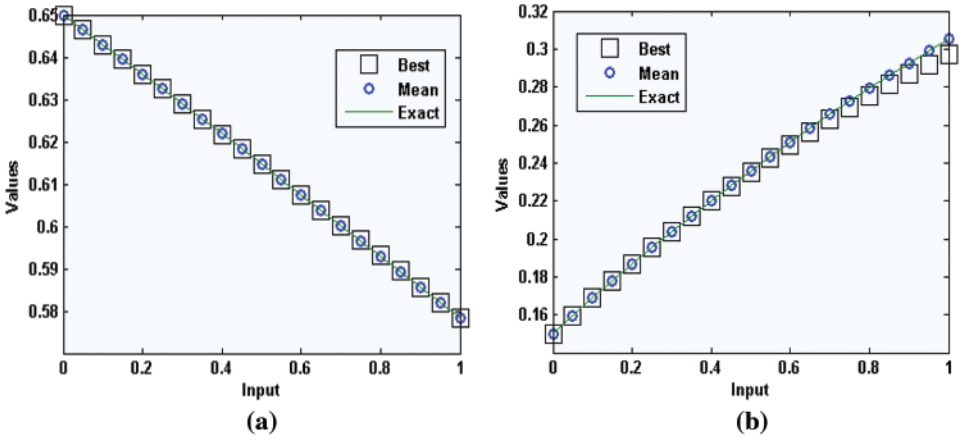

Figure 3: (Continued)

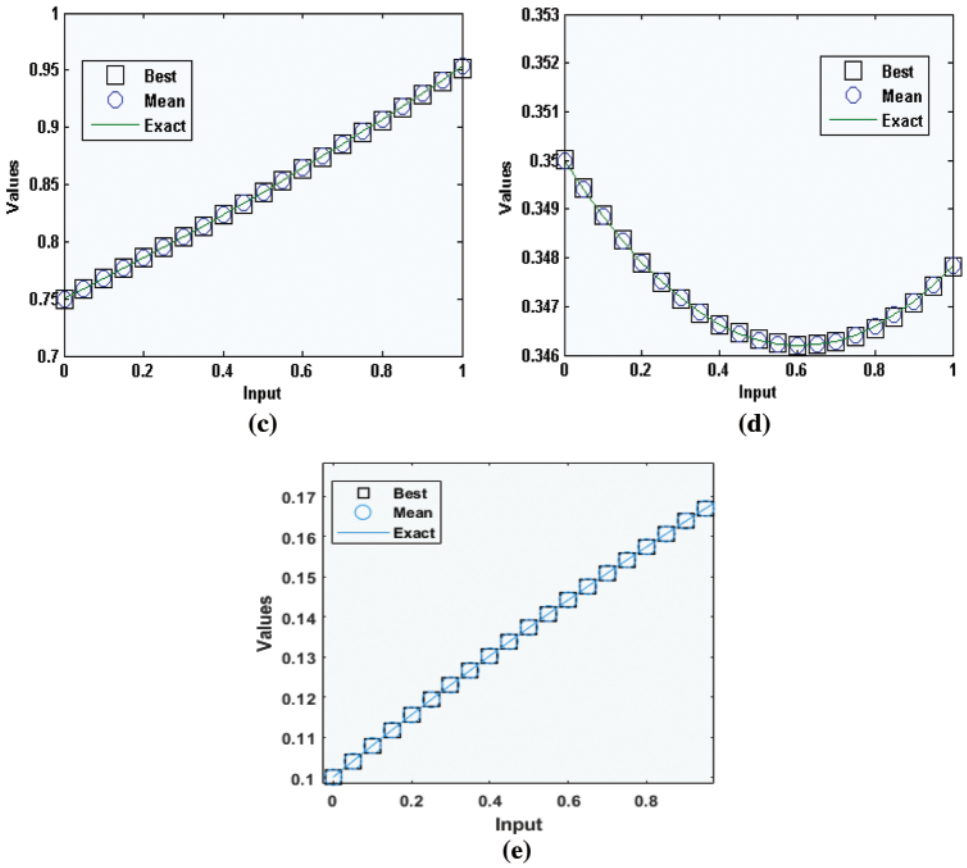

Figure 3: Result comparison for the SITR fractal system (a) Result comparison for the class S_1 (b) Result comparison for the class S_2 (c) Result comparison for the class I (d) Result comparison for the class T (e) Result comparison for the class R

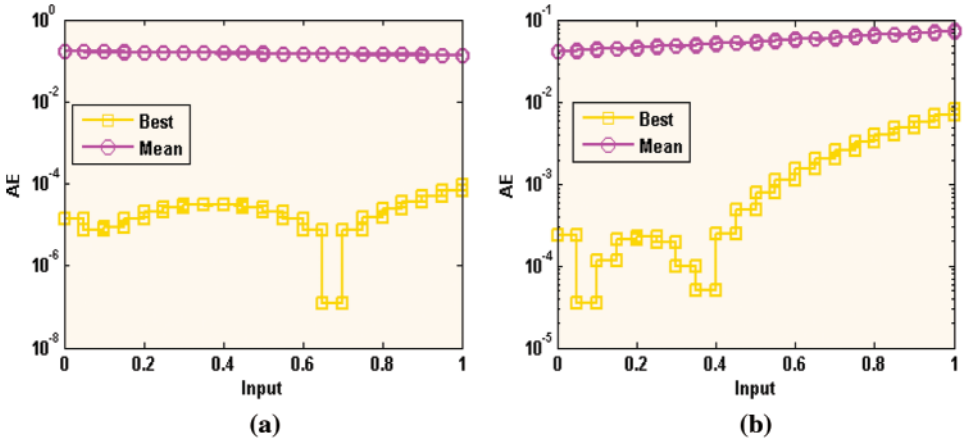

Figure 4: (Continued)

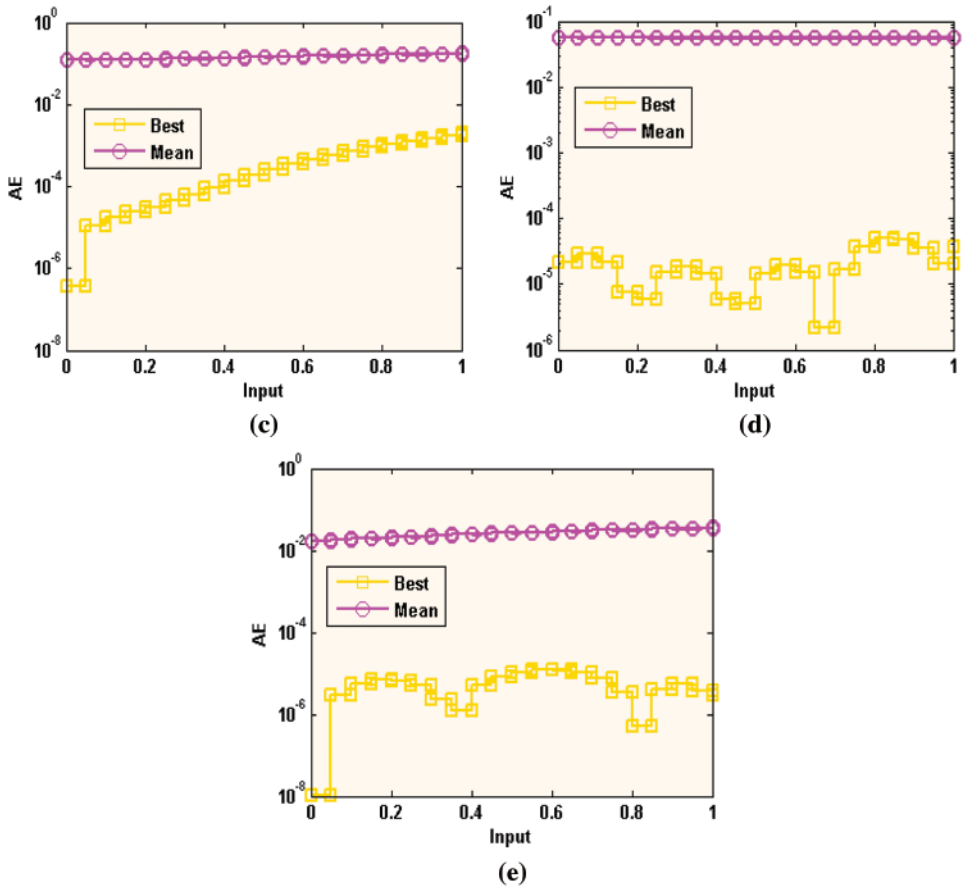

Figure 4: AE for the SITR fractal system (a) Mean and Best AE for class S_1 (b) Mean and Best AE for class S_2 (c) Mean and Best AE for class I (d) Mean and Best AE for class T (e) Mean and Best AE for class R

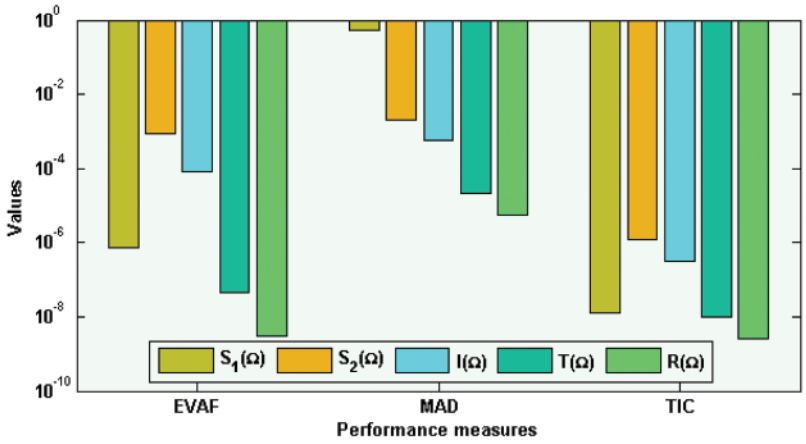

Figure 5: Performance measures for the SITR fractal system

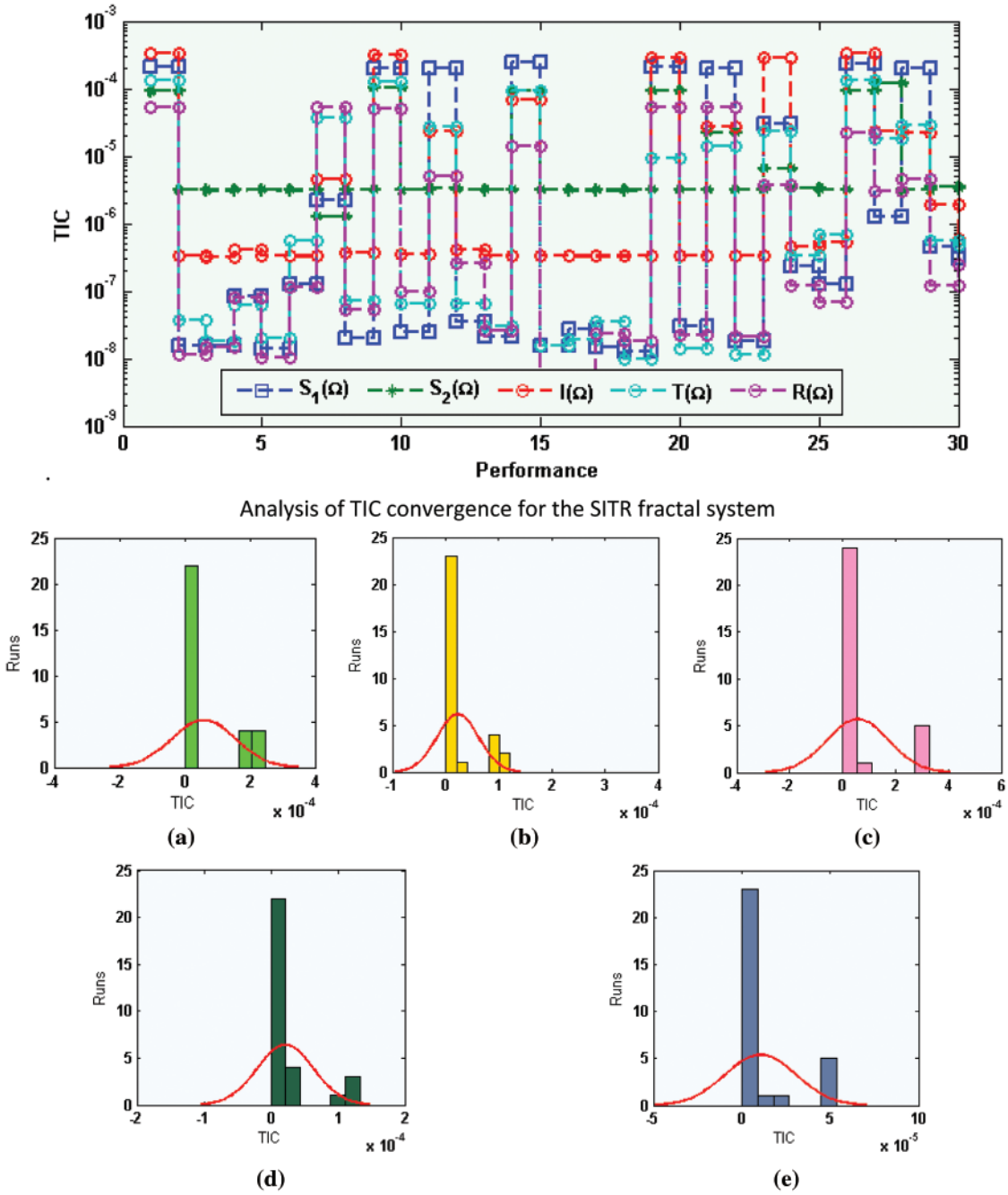

Figure 6: Convergence performance through TIC for the SITR fractal system along with histograms. (a) Hist for class S_1 (b) Hist for class S_2 (c) Hist for class I (d) Hist for class T (e) Hist for class R

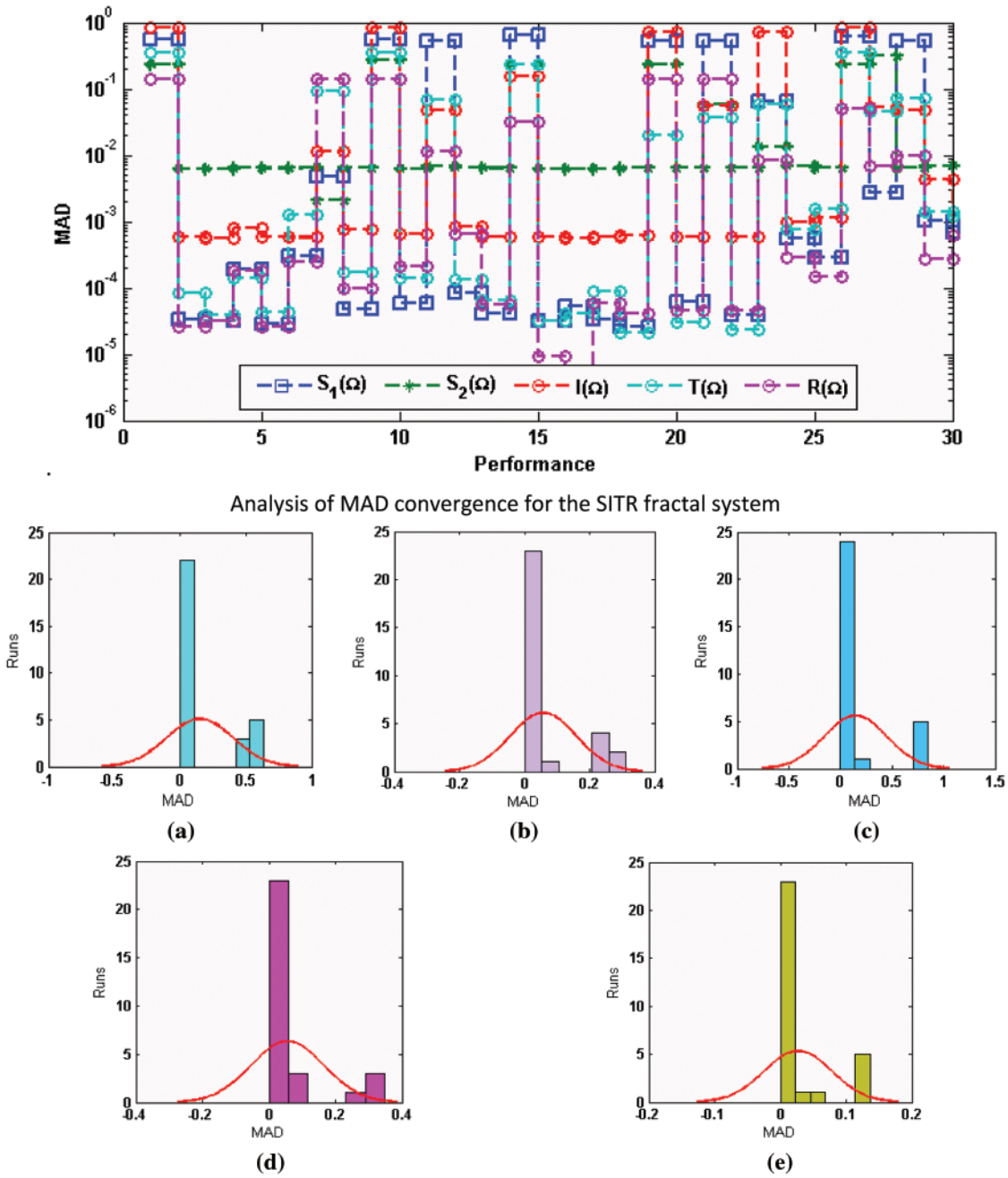

Figure 7: Convergence performance through MAD for the SITR fractal system along with histograms. (a) Hist for class S_1 (b) Hist for class S_2 (c) Hist for class I (d) Hist for class T (e) Hist for class R

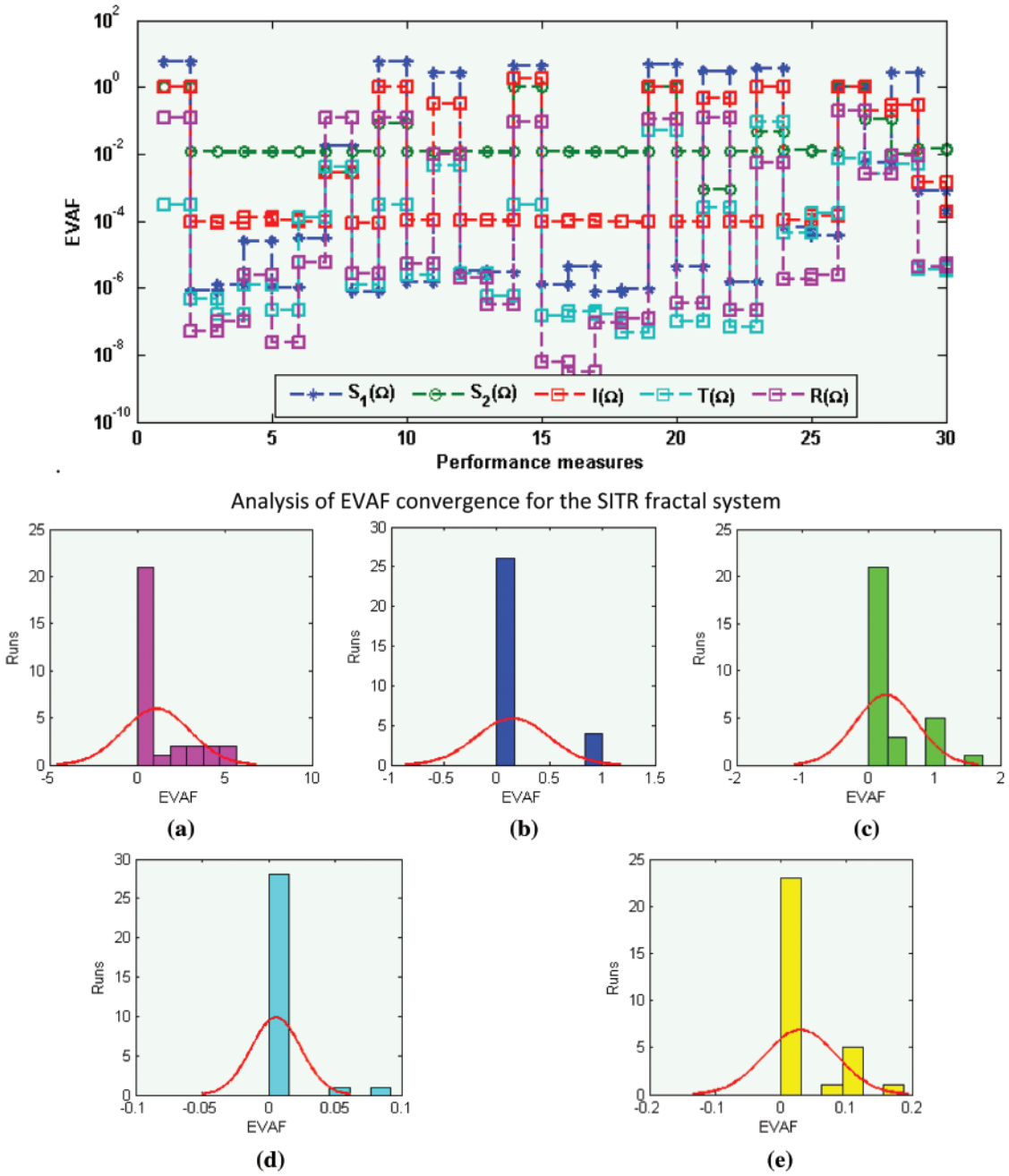

Figure 8: Convergence performance through EVAF for the SITR fractal system along with histograms. (a) Hist for class S_1 (b) Hist for class S_2 (c) Hist for class I (d) Hist for class T (e) Hist for class R

The performances of the statistical operatives based on TIC, MAD and EVAF is illustrated in Figs. 6–8. It is observed that the TIC performance for the corresponding categories of the coronavirus model found around 10^{-07}–10^{-08}, 10^{-05}–10^{-06}, 10^{-06}–10^{-08}, 10^{-07}–10^{-08} and 10^{-07}–10^{-09}. The MAD performance for the corresponding categories of the coronavirus model found around 10^{-03}–10^{-04}, 10^{-02}–10^{-03}, 10^{-02}–10^{-04}, 10^{-04}–10^{-05} and 10^{-03}–10^{-06}. The TIC performance for the corresponding categories of the coronavirus model is calculated as 10^{-04}–10^{-06}, 10^{-06}–10^{-07}, 10^{-04}–10^{-05}, 10^{-06}–10^{-08} and 10^{-06}–10^{-09}. These optimal small performances enhance the precision and worth of the method.

The performance measures for the SITR fractal system are plotted in Fig. 5. It can be observed that the EVAF performances for the corresponding classes of the model are calculated around 10^{-06}–10^{-07}, 10^{-02}–10^{-03}, 10^{-03}–10^{-04}, 10^{-07}–10^{-08} and 10^{-08}–10^{-09}. The MAD performances for the corresponding classes of the model are calculated around 10^{-01}–10^{-02}, 10^{-02}–10^{-04}, 10^{-03}–10^{-04}, 10^{-05}–10^{-06} and 10^{-06}–10^{-07}. Moreover, the TIC performances for the corresponding classes of the model are calculated around 10^{-08}–10^{-09}, 10^{-06}–10^{-07}, 10^{-07}–10^{-08}, 10^{-09}–10^{-10} and 10^{-09}–10^{-10}, respectively. It is concluded that the performance of these operators for solving the coronavirus model is accurate and stable.

For more precision and accuracy measures, the statistical representations of the SITR fractal system are provided for the corresponding classes lie around 10^{-06}–10^{-07}, 10^{-02}–10^{-03}, 10^{-03}–10^{-04}, 10^{-07}–10^{-08} and 10^{-08}–10^{-09}. The statistical results for the Minimum (Min), Mean, Maximum (Max), Median, standard deviation (STD) and semi-interquartile range (SIR) have been executed. The error analysis of the Min and Max values shows the best and worst runs, respectively. The S.I.R is half of the 3rd and 1st quartile. It is seen that the Min values for $S_1(\Omega)$, $S_2(\Omega)$, $I(\Omega)$, $T(\Omega)$ and $R(\Omega)$ lie around 10^{-05}–10^{-08}. The Max values are even worst runs lie around 10^{-01}–10^{-02} for each group of the SITR model. The Max values are even for worst runs lie around 10^{-01}–10^{-02} for each group of the SITR model. The Mean, S.I.R and STD for the SITR fractal system found around 10^{-01}–10^{-03}. However, the Median values for the r SITR fractal system found around 10^{-04}–10^{-05}. These consistent values authenticate the accuracy and stability of the designed method for the SITR fractal system.

5 Conclusions

This study aimsto exploit the Morlet wavelet neural networks using the numerical performances of the SITR fractal system-based coronavirus. An objective function using the differential system and initial conditions is formulated using the optimization computing strength of global and local search schemes of GA-ASA. The validation of the designed method is experiential through the comparison of the results. The absolute error values are also performed in good measures based on the nonlinear SITR fractal system. The performances of EVAF, MAD and TIC operators have been investigated in good measures for 15 variables to solve the SITR fractal system. The convergence performance through TIC, MAD and EVAF operators using MWNN-GA-ASA for 30 independent executions is also performed. One can prove that these measures prove good performances to solve the nonlinear SITR fractal system. The statistically based gages Min, Mean, Max, Median, STD and S.I.R are also performed in good ranges to solve each class of the SITR fractal model. On the behalf of these assessments, one can authenticate that the designed method is stable, precise and robust to solve the SITR fractal system.

This paper can be regarded as the continuation of the work of the authors contained in papers [51–53]. In the future, the proposed computational approach can be implemented to solve

the nonlinear models of a higher order [54–56], software-defined networks (SDN) models [57–64], and nonlinear fluids models [65–69].

Funding Statement: The authors extend their appreciation to the Deanship of Scientific Research at Imam Mohammad Ibn Saud Islamic University for funding this work through Research Group No. RG-21-09-12.

Conflicts of Interest: The authors declare that they have no conflicts of interest to report regarding the present study.

References

1. Gao, W., Baskonus, H. M., Shi, L. (2020). New investigation of bats-hosts-reservoir-people coronavirus model and application to 2019-nCoV system. *Advances in Difference Equations, 2020(1),* 448. DOI 10.1186/s13662-020-02831-6.
2. Umara, M., Sabir, Z., Raja, M. A. Z., Amin, F., Saeed, T. et al. (2021). Integrated neuro-swarm heuristic with interior-point for nonlinear SITR model for dynamics of novel COVID-19. *Alexandria Engineering Journal, 60(3),* 2811–2824. DOI 10.1016/j.aej.2021.01.043.
3. Khan, M. A., Atangana, A. (2020). Modeling the dynamics of novel coronavirus (2019-nCov) with fractional derivative. *Alexandria Engineering Journal, 59(4),* 2379–2389. DOI 10.1016/j.aej.2020.02.033.
4. Umara, M., Sabir, Z., Raja, M. A. Z., Shoai, M., Gupta, M. et al. (2020). A stochastic intelligent computing with neuro-evolution heuristics for nonlinear SITR system of novel COVID-19 dynamics. *Symmetry, 12(10),* 1628. DOI 10.3390/sym12101628.
5. Sánchez, Y. G., Sabir, Z., Guirao, J. L. (2020). Design of a nonlinear SITR fractal model based on the dynamics of a novel coronavirus (COVID-19). *Fractals, 28(8),* 2040026. DOI 10.1142/S0218348X20400265.
6. Sabir, Z., Guirao, J. L., Saeed, T. (2021). Solving a novel designed second order nonlinear Lane–Emden delay differential model using the heuristic techniques. *Applied Soft Computing, 102(3),* 107105. DOI 10.1016/j.asoc.2021.107105.
7. Guirao, J. L., Sabir, Z., Saeed, T. (2020). Design and numerical solutions of a novel third-order nonlinear Emden–Fowler delay differential model. *Mathematical Problems in Engineering, 2020(3),* 1–9. DOI 10.1155/2020/7359242.
8. Sabir, Z., Raja, M. A. Z., Shoai, M., Gupta, M. (2021). A novel design of fractional Meyer wavelet neural networks with application to the nonlinear singular fractional Lane-Emden systems. *Alexandria Engineering Journal, 60(2),* 2641–2659. DOI 10.1016/j.aej.2021.01.004.
9. Sabir, Z., Raja M., Baleanu D. (2021). Fractional mayer neuro-swarm heuristic solver for multi-fractional order doubly singular model based on Lane–Emden equation. *Fractals, 29(5),* 2140017–2141219. DOI 10.1142/S0218348X2140017X.
10. Sabir, Z., Raja, M. A. Z., Shoai, M., Aguilar, J. F. G. (2020). FMNEICS: Fractional meyer neuro-evolution-based intelligent computing solver for doubly singular multi-fractional order Lane–Emden system. *Computational and Applied Mathematics, 39(4),* 1866. DOI 10.1007/s40314-020-01350-0.
11. Sabir, Z., Raja, M. A. Z., Shoai, M., Gupta, M., Saeed, T. (2021). Meyer wavelet neural networks to solve a novel design of fractional order pantograph Lane-Emden differential model. *Chaos, Solitons & Fractals, 152(2),* 111404. DOI 10.1016/j.chaos.2021.111404.
12. Umar, M., Sabir, Z., Raja, M. A. Z. (2019). Intelligent computing for numerical treatment of nonlinear prey–predator models. *Applied Soft Computing, 80(S48),* 506–524. DOI 10.1016/j.asoc.2019.04.022.
13. Shoaib, M., Raja, M. A. Z., Jamshed, W., Nisar, K. S., Khan, I. et al. (2021). Intelligent computing Levenberg Marquardt approach for entropy optimized single-phase comparative study of second grade nanofluidic system. *International Communications in Heat and Mass Transfer, 127(1),* 105544. DOI 10.1016/j.icheatmasstransfer.2021.105544.

14. Awais, M., Bibi, M., Raja, M. A. Z., Awan, S. A., Malik, M. Y. (2021). Intelligent numerical computing paradigm for heat transfer effects in a Bodewadt flow. *Surfaces and Interfaces, 26(5),* 101321. DOI 10.1016/j.surfin.2021.101321.
15. Ahmad, I., Ilyas, H., Raja, M. A. Z., Khan, Z., Shoaib, M. (2021). Stochastic numerical computing with Levenberg-Marquardt backpropagation for performance analysis of heat Sink of functionally graded material of the porous fin. *Surfaces and Interfaces, 26(4),* 101403. DOI 10.1016/j.surfin.2021.101403.
16. Umar, M., Sabir, Z., Amin, F., Guirao, J. L. G., Raja, M. A. Z. (2020). Stochastic numerical technique for solving HIV infection model of $CD4^+$ T cells. *European Physical Journal Plus, 135(5),* 81. DOI 10.1140/epjp/s13360-020-00417-5.
17. Ilyas, H., Ahmad, I., Raja, M. A. Z., Tahir, M. B., Shoaib, M. (2021). Neuro-intelligent mappings of hybrid hydro-nanofluid Al_2O_3–Cu–H_2O model in porous medium over rotating disk with viscous dissolution and Joule heating. *International Journal of Hydrogen Energy, 46(55),* 28298–28326. DOI 10.1016/j.ijhydene.2021.06.065.
18. Shoaib, M., Raja, M. A. Z., Farhat, I., Shah, Z., Kumam, P. (2021). Soft computing paradigm for Ferrofluid by exponentially stretched surface in the presence of magnetic dipole and heat transfer. *Alexandria Engineering Journal, 61(2),* 1607–1623.
19. Sabir, Z., Raja, M. A. Z., Umar, M., Shoaib, M. (2020). Neuro-swarm intelligent computing to solve the second-order singular functional differential model. *European Physical Journal Plus, 135(6),* 1041. DOI 10.1140/epjp/s13360-020-00440-6.
20. Almalki, M. M., Alaidarous, E. S., Raja, M. A. Z., Maturi, D. A., Shoaib, M. (2021). Optimization through the Levenberg—Marquardt backpropagation method for a magnetohydrodynamic squeezing flow system. *Coatings, 11(7),* 779. DOI 10.3390/coatings11070779.
21. Raja, M. A. Z., Khan, Z., Zuhra, S., Ishtiaq, N., Wasim, K. et al. (2021). Cattaneo-christov heat flux model of 3D hall current involving biconvection nanofluidic flow with Darcy-Forchheimer law effect: Backpropagation neural networks approach. *Case Studies in Thermal Engineering, 26(6),* 101168. DOI 10.1016/j.csite.2021.101168.
22. Ahmad, I., Ahmad, S., Awais, M., Ahmad, S. U. I., Raja, M. A. Z. (2018). Neuro-evolutionary computing paradigm for Painlevé equation-II in nonlinear optics. *European Physical Journal Plus, 133(5),* 357. DOI 10.1140/epjp/i2018-12013-3.
23. Ilyas, H., Raja, M. A. Z., Ahmad, I., Shoaib, M. (2021). A novel design of Gaussian Wavelet Neural Networks for nonlinear Falkner-Skan systems in fluid dynamics. *Chinese Journal of Physics, 72(80),* 386–402. DOI 10.1016/j.cjph.2021.05.012.
24. Sabir, Z., Manzar, M. A., Raja, M. A. Z., Sheraz, M., Wazwaz, A. M. (2018). Neuro-heuristics for nonlinear singular Thomas-Fermi systems. *Applied Soft Computing, 65(6),* 152–169. DOI 10.1016/j.asoc.2018.01.009.
25. Uddin, I., Ullah, I., Raja, M. A. Z., Shoaib, M., Islam, S. et al. (2021). Design of intelligent computing networks for numerical treatment of thin film flow of Maxwell nanofluid over a stretched and rotating surface. *Surfaces and Interfaces, 24(5),* 101107. DOI 10.1016/j.surfin.2021.101107.
26. Umar, M., Raja, M. A. Z., Sabir, Z., Alwabli, A. S., Shoaib, M. (2020). A stochastic computational intelligent solver for numerical treatment of mosquito dispersal model in a heterogeneous environment. *European Physical Journal Plus, 135(7),* 378. DOI 10.1140/epjp/s13360-020-00557-8.
27. Ahmad, I., Raja, M. A. Z., Ramos, H., Bilal, M., Shoaib, M. (2021). Integrated neuro-evolution-based computing solver for dynamics of nonlinear corneal shape model numerically. *Neural Computing and Applications, 33(11),* 5753–5769. DOI 10.1007/s00521-020-05355-y.
28. Raja, M. A. Z., Umar, M., Sabir, Z., Khan, J. A., Baleanu, D. (2018). A new stochastic computing paradigm for the dynamics of nonlinear singular heat conduction model of the human head. *European Physical Journal Plus, 133(9),* S11. DOI 10.1140/epjp/i2018-12153-4.
29. Shoaib, M., Raja, M. A. Z., Khan, M. A. R., Farhat, I., Awan, S. E. (2021). Neuro-computing networks for entropy generation under the influence of MHD and thermal radiation. *Surfaces and Interfaces, 25(1),* 101243. DOI 10.1016/j.surfin.2021.101243.

30. Sabir, Z., Khalique, C. M., Raja, M. A. Z., Baleanu, D. (2021). Evolutionary computing for nonlinear singular boundary value problems using neural network, genetic algorithm and active-set algorithm. *European Physical Journal Plus, 136(2),* 129. DOI 10.1140/epjp/s13360-021-01171-y.
31. Sabir, Z., Raja, M. A. Z., Guirao, J. L., Shoaib, M. (2020). A neuro-swarming intelligence-based computing for second order singular periodic non-linear boundary value problems. *Frontiers in Physics, 8,* 1256. DOI 10.3389/fphy.2020.00224.
32. Sabir, Z., Wahab, H. A., Umar, M., Sakar, M. G., Raja, M. A. Z. (2020). Novel design of Morlet wavelet neural network for solving second order Lane–Emden equation. *Mathematics and Computers in Simulation, 172(27),* 1–14. DOI 10.1016/j.matcom.2020.01.005.
33. Majeed, K., Masood, Z., Samar, R., Raja, M. A. Z. (2017). A genetic algorithm optimized Morlet wavelet artificial neural network to study the dynamics of nonlinear Troesch's system. *Applied Soft Computing, 56(8),* 420–435. DOI 10.1016/j.asoc.2017.03.028.
34. Sabir, Z., Nisar, K., Raja, M. A. Z., Ibrahim, A. A. B. A., Rodrigues, J. J. P. C. et al. (2021). Design of Morlet wavelet neural network for solving the higher order singular nonlinear differential equations. *Alexandria Engineering Journal, 60(6),* 5935–5947. DOI 10.1016/j.aej.2021.04.001.
35. Maleki, N., Zeinali, Y., Niaki, S. T. A. (2021). A k-NN method for lung cancer prognosis with the use of a genetic algorithm for feature selection. *Expert Systems with Applications, 164(5),* 113981. DOI 10.1016/j.eswa.2020.113981.
36. Liang, H., Zou, J., Zuo, K., Khan, M. J. (2020). An improved genetic algorithm optimization fuzzy controller applied to the wellhead back pressure control system. *Mechanical Systems and Signal Processing, 142,* 106708. DOI 10.1016/j.ymssp.2020.106708.
37. Mehmood, A., Zameer, A., Ling, S. H., Rehman, A., Raja, M. A. Z. (2020). Integrated computational intelligent paradigm for nonlinear electric circuit models using neural networks, genetic algorithms and sequential quadratic programming. *Neural Computing and Applications, 32(14),* 10337–10357. DOI 10.1007/s00521-019-04573-3.
38. Sabir, Z., Nisar, K., Raja, M. A. Z., Haque, M. R., Umar, M. et al. (2021). IoT technology enabled heuristic model with Morlet wavelet neural network for numerical treatment of heterogeneous mosquito release ecosystem. *IEEE Access, 9,* 132897–132913. DOI 10.1109/ACCESS.2021.3113986.
39. Raja, M. A. Z., Aslam, M. S., Chaudhary, N. I., Nawaz, M., Shah, S. M. (2019). Design of hybrid nature-inspired heuristics with application to active noise control systems. *Neural Computing and Applications, 31(7),* 2563–2591. DOI 10.1007/s00521-017-3214-2.
40. Sabir, Z., Raja, M. A. Z., Guirao, J. L., Saeed, T. (2021). Solution of novel multi-fractional multi-singular Lane–Emden model using the designed FMNEICS. *Neural Computing and Applications, 33(24),* 17287–17302. DOI 10.1007/s00521-021-06318-7.
41. do Valle Tomaz, I., Colaço, F. H. G., Sarfraz, S., Pimenov, D. Y., Gupta, M. K. et al. (2021). Investigations on quality characteristics in gas tungsten arc welding process using artificial neural network integrated with genetic algorithm. *The International Journal of Advanced Manufacturing Technology, 113(11),* 3569–3583.
42. Chen, F., Xu, S., Zhao, Y., Zhang, H. (2020). An adaptive genetic algorithm of adjusting sensor acquisition frequency. *Sensors, 20(4),* 990. DOI 10.3390/s20040990.
43. Zameer, A., Majeed, M., Mirza, S. M., Raja, M. A. Z., Khan, A. et al. (2019). Bio-inspired heuristics for layer thickness optimization in multilayer piezoelectric transducer for broadband structures. *Soft Computing, 23(10),* 3449–3463. DOI 10.1007/s00500-017-3002-z.
44. Sabir, Z., Amin, F., Pohl, D., Guirao, J. L. (2020). Intelligence computing approach for solving second order system of Emden–Fowler model. *Journal of Intelligent & Fuzzy Systems, 38(6),* 7391–7406. DOI 10.3233/JIFS-179813.
45. Gao, Y., Song, H., Wang, X., Zhang, K. (2020). Primal-dual active set method for pricing American better-of option on two assets. *Communications in Nonlinear Science and Numerical Simulation, 80,* 104976. DOI 10.1016/j.cnsns.2019.104976.
46. Li, Y., Yuan, G., Sheng, Z. (2018). An active-set algorithm for solving large-scale nonsmooth optimization models with box constraints. *PLoS One, 13(1),* e0189290. DOI 10.1371/journal.pone.0189290.

47. Burdakov, O., Sysoev, O. (2017). Primal-dual active set strategy for large scale optimization of cardiac defibrillation. *Applied Mathematics and Computation, 292(7),* 178–193. DOI 10.1016/j.amc.2016.07.035.
48. Chamakuri, N., Kunisch, K. (2017). Primal-dual active set strategy for large scale optimization of cardiac defibrillation. *Applied Mathematics and Computation, 292,* 178–193.
49. Gilbert, A. D., Wasilkowski, G. W. (2017). Small superposition dimension and active set construction for multivariate integration under modest error demand. *Journal of Complexity, 42,* 94–109. DOI 10.1016/j.jco.2017.03.001.
50. Nak, H., Akkaya, Ş., Yumuk, E. (2017). Active set method based model predictive control for a ball and beam system. *10th International Conference on Electrical and Electronics Engineering* , pp. 871–875. Bursa, Turkey.
51. Wang, S. H., Govindaraj, V. V., Górriz, J. M., Zhang, X., Zhang, Y. D. (2021). COVID-19 classification by FGCNet with deep feature fusion from graph convolutional network and convolutional neural network. *Information Fusion, 67,* 208–229. DOI 10.1016/j.inffus.2020.10.004.
52. Wang, S. H., Nayak, D. R., Guttery, D. S., Zhang, X., Zhang, Y. D. (2021). COVID-19 classification by CCSHNet with deep fusion using transfer learning and discriminant correlation analysis. *Information Fusion, 68(2),* 131–148. DOI 10.1016/j.inffus.2020.11.005.
53. Wang, S. H., Fernandes, S., Zhu, Z., Zhang, Y. D. (2021). AVNC: Attention-based VGG-style network for COVID-19 diagnosis by CBAM. *IEEE Sensors Journal,* 1. DOI 10.1109/JSEN.2021.3062442.
54. Sabir, Z., Raja, M. A. Z., Guirao, J. L., Shoaib, M. (2020). Integrated intelligent computing with neuro-swarming solver for multi-singular fourth-order nonlinear Emden–Fowler equation. *Computational and Applied Mathematics, 39(4),* 4. DOI 10.1007/s40314-020-01330-4.
55. Sabir, Z., Saoud, S., Raja, M. A. Z., Wahab, H. A., Arbi, A. (2020). Heuristic computing technique for numerical solutions of nonlinear fourth order Emden–Fowler equation. *Mathematics and Computers in Simulation, 178(7),* 534–548. DOI 10.1016/j.matcom.2020.06.021.
56. Sabir, Z., Sakar, M. G., Yeskindirova, M., Saldir, O. (2020). Numerical investigations to design a novel model based on the fifth order system of Emden–Fowler equations. *Theoretical and Applied Mechanics Letters, 10(5),* 333–342. DOI 10.1016/j.taml.2020.01.049.
57. Haider, I., Khan, K. B., Haider, M. A., Saeed, A., Nisar, K. (2020). Automated robotic system for assistance of isolated patients of coronavirus (COVID-19). *IEEE 23rd International Multitopic Conference, 1–6*. Bahawalpur, Pakistan.
58. Hovav, S., Tsadikovich, D. (2015). A network flow model for inventory management and distribution of influenza vaccines through a healthcare supply chain. *Operations Research for Health Care, 5(2),* 49–62. DOI 10.1016/j.orhc.2015.05.003.
59. Haque, M. R., Tan, S. C., Yusoff, Z., Lee, C. K., Kaspin, R. (2019). DDoS attack monitoring using smart controller placement in software defined networking architecture. *Computational Science and Technology, 481,* 195–203. DOI 10.1007/978-981-13-2622-6.
60. Sarkar, N. I., Kuang, A. X. M., Nisar, K., Amphawan, A. (2014). Performance studies of integrated network scenarios in a hospital environment. *International Journal of Information Communication Technologies and Human Development, 6(1),* 35–68. DOI 10.4018/IJICTHD.
61. Sarkar, N. I., Kuang, A. X. M., Nisar, K., Amphawan, A. (2014). Hospital environment scenarios using WLAN over OPNET simulation tool. *International Journal of Information Communication Technologies and Human Development, 6(1),* 69–90. DOI 10.4018/IJICTHD.
62. Chowdhry, B. S., Shah, A. A., Harris, N., Hussain, T., Nisar, K. (2020). Development of a smart instrumentation for analyzing railway track health monitoring using forced vibration. *IEEE 14th International Conference on Application of Information and Communication Technologies (AICT)*, pp. 1–5. Tashkent, Uzbekistan.
63. Nisar, K. (2018). Smart home: Multisensor information fusion towards better healthcare. *Advanced Science Letters, 24(3),* 1896–1901.
64. Patel, R., Longini Ira, M., Halloran, M. E. (2005). Finding optimal vaccination strategies for pandemic influenza using genetic algorithms. *Journal of Theoretical Biology, 234(2),* 201–212. DOI 10.1016/j.jtbi.2004.11.032.

65. Raja, M. A. Z., Ahmed, T., Shah, S. M. (2017). Intelligent computing strategy to analyze the dynamics of convective heat transfer in MHD slip flow over stretching surface involving carbon nanotubes. *Journal of the Taiwan Institute of Chemical Engineers, 80(3),* 935–953. DOI 10.1016/j.jtice.2017.08.016.
66. Mehmood, A., Afsar, K., Zameer, A., Awan, S. E., Raja, M. A. Z. (2019). Integrated intelligent computing paradigm for the dynamics of micropolar fluid flow with heat transfer in a permeable walled channel. *Applied Soft Computing, 79(9),* 139–162. DOI 10.1016/j.asoc.2019.03.026.
67. Ahmad, I., Zahid, H., Ahmad, F., Raja, M. A. Z., Baleanu, D. (2019). Design of computational intelligent procedure for thermal analysis of porous fin model. *Chinese Journal of Physics, 59(4),* 641–655. DOI 10.1016/j.cjph.2019.04.015.
68. Shoaib, M., Raja, M. A. Z., Sabir, M. T., Islam, S., Shah, Z. et al. (2020). Numerical investigation for rotating flow of MHD hybrid nanofluid with thermal radiation over a stretching sheet. *Scientific Reports, 10(1),* 551. DOI 10.1038/s41598-020-75254-8.
69. Umar, M., Sabir, Z., Imran, A., Wahab, A. H., Shoaib, M. et al. (2020). The 3-D flow of Casson nanofluid over a stretched sheet with chemical reactions, velocity slip, thermal radiation and Brownian motion. *Thermal Science, 24(5),* 2929–2939. DOI 10.2298/TSCI190625339U.